SINTEF
PROCEEDINGS 6

14th International Conference on CFD in
Oil & Gas, Metallurgical and Process Industries
SINTEF, Trondheim, Norway, October 12–14, 2020

Proceedings from the 14th International Conference on CFD in Oil & Gas, Metallurgical and Process Industries

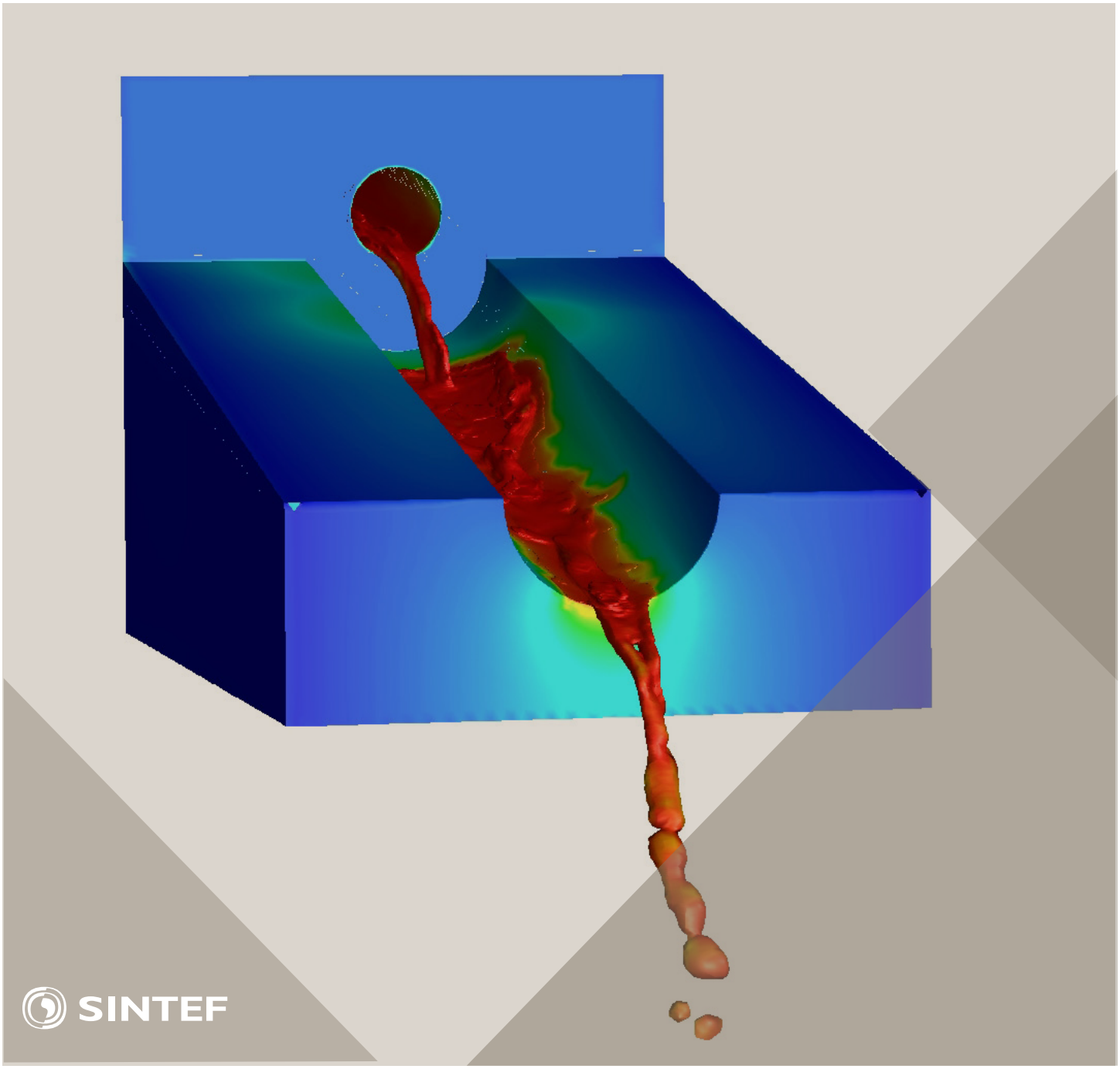

SINTEF Proceedings

Editors:
Jan Erik Olsen, Jan Hendrik Cloete and Stein Tore Johansen

Proceedings from the 14th International Conference on CFD in Oil & Gas, Metallurgical and Process Industries

SINTEF, Trondheim, Norway
October 12–14, 2020

SINTEF Academic Press

SINTEF Proceedings 6
Editors: Jan Erik Olsen, Jan Hendrik Cloete and Stein Tore Johansen

Proceedings from the 14th International Conference on CFD in Oil & Gas, Metallurgical and Process Industries, SINTEF, Trondheim, Norway, October 12–14, 2020

Keywords:
CFD, fluid dynamics, modelling

Cover illustration: Tapping of metal by Jan Erik Olsen

ISSN 2387-4295 (online)
ISBN 978-82-536-1684-1 (pdf)

SINTEF Academic Press
Address: Børrestuveien 3
PO Box 124 Blindern
N-0314 OSLO
Tel: +47 40 00 51 00

www.sintef.no/community
www.sintefbok.no

14th International Conference on CFD in Oil & Gas, Metallurgical and Process Industries
SINTEF, Trondheim, NORWAY
October 12-14, 2020

VOLUME-OF-FLUID SIMULATION OF GAS DISSOLUTION IN LIQUID: RISING BUBBLES AND CO_2 TRAPPING

Alexandros PATSOUKIS-DIMOU[1], **Julien MAES**[1*]

[1]Institute of GeoEnergy Engineering, Heriot-Watt University, Edinburgh EH14 4AS, UK

* E-mail: j.maes@hw.ac.uk

ABSTRACT

Multiphase multispecies transport is an essential field of study for a wide range of applications including bubble reactors and CO_2 storage in the subsurface. Modelling of these processes is challenging due to the discontinuity of material properties, making accurate modelling of mass transfer at reactive interface difficult. Maes and Soulaine (2020) have recently developed a numerical model based on a single-field formulation for Volume-Of-Fluid simulation of interfacial mass transfer with local volume changes. This model was validated by comparison with a semi-analytical solution for the dissolution of a rising bubble of gas in liquid in the creeping (or spherical) flow regime. However, this model is only first-order accurate, and will therefore depend strongly on the discretization scheme used. In this work, we consider two different numerical schemes for the discretization of species interfacial fluxes. Convergence and accuracy are compared for dissolution of a rising bubble of gas in liquid at various regimes (spherical, ellipsoidal shape and dimpled ellipsoidal shaped). The model is then applied to simulate the dissolution of trapped bubble of CO_2 in a cavity.

Keywords: Interface, mass transfer, Volume-Of-Fluid, rising bubbles, CO_2 .

NOMENCLATURE

Greek Symbols

α	phase volume fraction $[-]$
κ	interface curvature $[m^{-1}]$
μ	viscosity $[Pa.s]$
Φ	flux $[kg/m^2 s]$
ρ	Mass density, $[kg/m^3]$
σ	interfacial tension $[N/m]$
τ	viscous stress $[kg/m.s^2]$

Latin Symbols

A	area $[m^2]$
c	concentration $[kg/m^3]$
D	molecular diffusivity $[m^2/s]$
F	advective flux $[kg/m^2.s]$
f	interior force $[N/m^3]$
g	gravity accelaration $[m^2/s]$
H	Henry constant $[-]$
J	molecular diffusion flux $[k/m^2.s]$
L	reference length $[m]$
p	pressure $[Pa]$
t	time $[s]$
u	velocity $[m/s]$
U	reference velocity $[m/s]$

Sub/superscripts

Σ	fluid/fluid interface
g	gas phase.
l	liquid phase.

INTRODUCTION

Interface species transfers are present in a wide range of applications such as bubble column reactors and geological storage of CO_2 in aquifers. Experimental investigations can provide insights into the physics of these processes (Francois *et al.*, 2011; Roman *et al.*, 2016, 2019). However, it is often difficult to investigate a wide range of physical conditions experimentally, due to time and safety constraints. In addition, quantities (e.g. concentration, pH, interfacial flux) are difficult to measure during the course of the experiment. Computational Fluid Dynamics can be an essential tool to complement experiments and perform sensitivity analysis with physical parameters (Deising *et al.*, 2018; Maes and Geiger, 2018; Soulaine *et al.*, 2018).

Numerical simulation of two-phase flow can be performed using the algebraic Volume-Of-Fluid method (Ubbink and Issa, 1999) for which the interface between the two fluids is captured using an indicator function, which is a phase volume fraction. This indicator function is transported by numerically solving an advection equation.

Interface transfer can be modelled within the VOF method by using the single-field approach, developed by (Haroun *et al.*, 2010) and at the base of the Continuous Species Transfer (CST) method, later developed by (Marschall *et al.*, 2012). In the single-field approach, a mixture quantity, obtained by volume averaging of species concentration, is transported by solving an algebraic equation (Haroun *et al.*, 2010; Deising *et al.*, 2016).

The method has recently been extended to include local volume change in order to simulate gas dissolution in liquid, and has been applied to simulate the dissolution of a rising gas bubble in liquid (Maes and Soulaine, 2020). However, this model is only first-order accurate, and will therefore depend strongly on the discretization scheme used. In this work, we consider two different numerical schemes for the discretization of species interfacial fluxes, which require an interpolation of the concentration in each phase from the center of

computational cells to the center of cell faces. In the Gauss linear scheme, the concentration in each phase is obtained by linear interpolation. In the phase upwinding scheme, the concentrations are calculated using upwinding based on the normal of the interface, so that each concentration is calculated in its own phase. Convergence and accuracy are compared for dissolution of a rising bubble of gas in liquid at various regimes (spherical, ellipsoidal shape and dimpled ellipsoidal shaped). The model is then applied to simulate the dissolution of a trapped bubble of CO_2 in a cavity.

MODEL DESCRIPTION

The model is described in detail in Maes and Soulaine (2020) and is summarized here.

The Volume-Of-Fluid Method

In the Volume-Of-Fluid method, the location of the interface is given by the indicator function α, which is equal to the volume fraction of one phase (here the liquid phase) in each grid cell. The density ρ and viscosity μ of the fluid are given by volume-averaging

$$\rho = \rho_l \alpha + \rho_g \left(1 - \alpha\right), \tag{1}$$

$$\mu = \mu_l \alpha + \mu_g \left(1 - \alpha\right), \tag{2}$$

where the subscripts l and g refer to the liquid and gas phase, respectively. The indicator function obeys

$$\frac{\partial \alpha}{\partial t} + \nabla \cdot \left(\alpha \mathbf{u}\right) + \nabla \cdot \left(\alpha \left(1 - \alpha\right) \mathbf{u}_r\right) = \frac{\dot{m}}{\rho_l}, \tag{3}$$

where $\dot{m}$ is the phase mass transfer rate and where $\mathbf{u}_r = \mathbf{u}_l - \mathbf{u}_g$ is the relative velocity, often assumed equal to zero. However, in order to reduce the smearing of the interface due to numerical diffusion, it is often replaced by a compressive velocity $\mathbf{u}_{comp}$, normal to the interface and with an amplitude based on the maximum of the single-field velocity (Rusche, 2002)

$$\mathbf{u}_r \equiv \mathbf{u}_{comp} = \overline{\mathbf{n}}_\Sigma \left[\min\left(c_\alpha \frac{|\phi_f|}{A_f}, \max_f\left(\frac{|\phi_f|}{A_f}\right)\right)\right], \tag{4}$$

where c_α is the compression constant (generally between 0 and 4) and ϕ_f is the volumetric flux across f. In all our simulations, we choose $c_\alpha = 1.0$.

The two fluids are assumed to be Newtonian and incompressible. Under isothermal condition and assuming constant interfacial tension, the single-field volume-averaged velocity field $\mathbf{u}$ and pressure p satisfies the single-field Navier-Stokes equations (Fleckenstein and Bothe, 2015)

$$\nabla \cdot \mathbf{u} = \dot{m} \left(\frac{1}{\rho_l} - \frac{1}{\rho_g}\right). \tag{5}$$

$$\frac{\partial \rho \mathbf{u}}{\partial t} + \nabla \cdot \left(\rho \mathbf{u}\mathbf{u}\right) = -\nabla p + \nabla \cdot \boldsymbol{\tau} + \rho \mathbf{g} + \mathbf{f}_\Sigma, \tag{6}$$

where $\mathbf{g}$ is the gravity vector, $\boldsymbol{\tau}$ is the viscous stress tensor and $\mathbf{f}_\sigma$ is the surface tension force. The viscous stress tensor can be expresses as

$$\boldsymbol{\tau} = \mu \left(\nabla \mathbf{u} + \nabla \mathbf{u}^T\right). \tag{7}$$

The Reynolds number is defined as the ratio of inertial to viscous forces

$$R_e = \frac{\rho_l L U}{\mu_l}, \tag{8}$$

where L and U are the reference length and velocity in the domain, and ρ and μ are the density and viscosity of the invading phase. The Reynolds number is used to characterise different flow regimes, such as laminar flow, where viscous forces are dominant, and turbulent flow, where inertial forces are dominant. The surface tension force can be modelled using the Continuum Surface Force (CSF) formulation introduced by Brackbill *et al.* (1992)

$$\mathbf{f}_\Sigma = \sigma \kappa \nabla \alpha. \tag{9}$$

where σ is the interfacial tension between the two fluids and κ the mean interface curvature, which can be computed as

$$\kappa = -\nabla \cdot \mathbf{n}_\Sigma, \tag{10}$$

where $\mathbf{n}_\Sigma$ is the interface normal vector, defined as

$$\mathbf{n}_\Sigma = \frac{\nabla \alpha}{||\nabla \alpha||}. \tag{11}$$

The relative importance of viscous forces, gravity and surface tension force is characterised using the Eötvös Eo and Morton Mo numbers,

$$\mathrm{Eo} = \frac{\Delta \rho g L^2}{\sigma}, \tag{12}$$

$$\mathrm{Mo} = \frac{g \mu_l^4 \Delta \rho}{\rho_l^2 \sigma^3}. \tag{13}$$

In case gravity has no impact, the relative importance of viscous and surface tension forces is characterised using the capillar number Ca

$$\mathrm{Ca} = \frac{\mu_l U}{\sigma}. \tag{14}$$

The Continuous Species Transfer Method

In this work, the gas phase is always assumed pure. In addition, we assume that the gas component dissolves in the liquid phase with Henry's constant H and remains diluted. In this case, the single-field concentration in the domain satisfies an advection-diffusion equation given by the Continuous Species Transfer (CST) formulation (Haroun *et al.*, 2010; Marschall *et al.*, 2012; Deising *et al.*, 2016)

$$\frac{\partial c}{\partial t} + \nabla . \mathbf{F} + \nabla . \mathbf{J} = 0, \tag{15}$$

where $\mathbf{F}$ is the advective flux and $\mathbf{J}$ is the diffusive flux. In order to maintain consistency between advection operators, the advective flux of the species is also modelled with a compressive velocity, using the normal Compressive CST (C-CST) formulation (Maes and Soulaine, 2020)

$$\mathbf{F} = c\mathbf{u} + \alpha \left(1 - \alpha\right) \frac{\nabla c \cdot \nabla \alpha}{||\nabla \alpha||^2} \mathbf{u}_{comp}. \tag{16}$$

For the diffusive flux, Maes and Soulaine (2020) showed that it can be written as

$$\mathbf{J} = -D^{SF} \nabla c + \boldsymbol{\Phi}, \tag{17}$$

where

$$\boldsymbol{\Phi} = (1 - H) D^{SF} \frac{c}{\alpha + H\left(1 - \alpha\right)} \nabla \alpha. \tag{18}$$

and D^{SF} is the single-field diffusion coefficient. The debate regarding the best formulation for the single-field diffusion

coefficient was initiated in the original work of Haroun *et al.* (2010) and pursued in Marschall *et al.* (2012) and Deising *et al.* (2016). Indeed, Haroun *et al.* (2010) first proposed an arithmetic mean for the diffusion coefficient

$$D^{SF} \equiv D^{a} = \alpha D_l + (1-\alpha) D_g. \tag{19}$$

However, Deising *et al.* (2016) performed a rigorous derivation of the single-field formulation with an arithmetic coefficient and show that additional terms arise, resulting from the discontinuity and curvature effect at the interface. They also show that Equ. (17) is correct if using a harmonic mean for the diffusion coefficient

$$D^{SF} \equiv D^{h} = \frac{1}{\frac{\alpha}{D_l} + \frac{1-\alpha}{D_g}}, \tag{20}$$

provided the additional assumption that the concentration in the gas bubble remains approximatively constant. However, this formulation can not be applied when $D_g = 0$, for example when the gas phase is pure. Instead, Maes and Soulaine (2020) shows that Equ. (17) is equivalent to the rigorous single-field formulation based on the arithmetic mean derived by Deising *et al.* (2016) if using the equilibrium-based mean diffusion

$$D^{SF} \equiv D^{e} = \frac{\alpha D_l + H(1-\alpha) D_g}{\alpha + H(1-\alpha)}. \tag{21}$$

The equilibrium-based mean diffusion has two advantages compared to the harmonic mean. First, it does not require the additional assumption that the concentration in the gas bubble remains approximatively constant, and second, it can be applied when $D_g = 0$.
Finally, the phase mass transfer rate at the interface where $0 < \alpha < 1$ can be calculated as (Maes and Soulaine, 2020)

$$\dot{m} = -\frac{D^e \nabla c - \mathbf{\Phi}}{1-\alpha} \cdot \nabla \alpha. \tag{22}$$

Numerical implementation

The numerical method has been implemented in GeoChemFoam (https://julienmaes.com/geochemfoam), our OpenFOAM®-based (OpenCFD, 2016) reactive transport solver. The full solution procedure is presented in Maes and Soulaine (2020). The standard VOF solver of OpenFOAM®, so-called *interFoam*, has been extended for this purpose into another solver called *interTransferFoam*. *interFoam* solves the system formed by Eq. (5), (3) and (6) on a collocated Eulerian grid. A pressure equation is obtained by combining the continuity (Eq. (5)) and momentum (Eq. (6)) equations. The system is then solved with a predictor-corrector strategy based on the Pressure Implicit Splitting Operator (PISO) algorithm (Issa *et al.*, 1985). Three iterations of the PISO loop are used to stabilise the system. An explicit formulation is used to treat the coupling between the phase distribution equation (Eq. (3)) and the pressure equation. This imposes a limit on the time-step size by introducing a capillary wave time scale described by the Brackbill conditions (Brackbill *et al.*, 1992).
In *interTransferFoam*, the concentration equation (Eq. (15)) is solved sequentially before the phase conservation. The interfacial mass transfer (Eq. (22)) is then computed and re-injected in the continuity (Eq. (5)) and phase equations (Eq. (3)). The space discretization of the convection terms is performed using the second-order *vanLeer* scheme (van Leer, 1974). For the compression terms, the interpolation of $\alpha_d \alpha_c$ is performed using the *interfaceCompression* scheme (OpenCFD, 2016). The diffusion term $\nabla.(D^e \nabla c)$ is discretized using the Gauss linear limited corrected scheme, which is second order and conservative. For the discretization of the CST flux, two different schemes are considered, the Gauss Linear (GL) scheme

$$\Phi_{GL} = D_f^e (1-H) \frac{c_f}{\alpha_f + H(1-\alpha_f)} \nabla \cdot \alpha \tag{23}$$

where D_f^e,c_f and α_f are the molecular diffusion, species concentration and phase volume fraction at face center obtained by linear interpolation, respectively and the Gauss Phase Upwinding scheme (GPU)

$$\Phi_{GPU} = \Phi_U - \Phi_D \tag{24}$$

where

$$\Phi_{Up} = D_f^e \frac{c_{Up}}{\alpha_{Up} + H(1-\alpha_{Up})} \cdot \nabla \alpha, \tag{25}$$

and

$$\Phi_{Dw} = H D_f^e \frac{c_{Dw}}{\alpha_{Dw} + H(1-\alpha_{Dw})} \cdot \nabla \alpha, \tag{26}$$

and c_{Up}, α_{Up}, c_{Dw} and α_{Dw} are the species concentration and phase volume fraction from the upstream and downstream cell in the direction of $\nabla \cdot \alpha$.
For the computation of the mass transfer $\dot{m}$, we define

$$\mathbf{\Phi}_D = \frac{D_f^e \nabla c - \mathbf{\Phi}}{1-\alpha} \tag{27}$$

and then we use

$$\mathbf{\Phi}_D \cdot \nabla \alpha = \nabla \cdot (\mathbf{\Phi}_D \alpha_{Dw}) - \alpha \nabla \cdot \mathbf{\Phi}_D. \tag{28}$$

This is only first-order accurate (Maes and Soulaine, 2020), but all second-order discretization schemes available in OpenFOAM® have shown strong instabilities. Due to this, the numerical results will be strongly impacted by the discretization scheme used for $\mathbf{\Phi}$. In this work, we will compare results obtained with the Gauss Linear and the Gauss Phase Upwinding schemes. The linear scheme is available in OpenFOAM® and the phase upwinding scheme has been implemented in GeoChemFoam (https://julienmaes.com/geochemfoam).

RESULTS

Rising bubbles

The objective of this section is to compare convergence and accuracy of the numerical model when using the linear or the phase upwinding schemes. For this we consider the dissolution of a rising single-component gas bubble immersed in liquid for three different regimes. The fluid roperties are summarized in Table 1.
For test case 1, a bubble with initial radius $R = 2$ mm is immersed in liquid 1 (Table 1) in a computational domain of dimension 1.2 cm × 2.4 cm × 1.2 cm. Symmetry conditions are applied to the plane x=0 and z=0, so only a quarter of the bubble is simulated. The other boundary conditions are free-flow. The flow properties correspond to an Eötvös number Eo=3.25 and a Morton number Mo=1.63. For these values, Clift's diagram describing the shape regime (Clift *et al.*, 1978) predicts a spherical shape. Initially, the centre of the bubble is placed at (0 mm, 3 mm, 0 mm). In order to compare

	Density (kg/m^3)	Dynamic viscosity (Pa.s)	Diffusivity (m^2/s)	Interfacial tension (liquid-gas) (mN/m)	Henry's constant (no unit)
Gas	1.2	1.8×10^{-5}	0		
Liquid 1	1245	0.46	1.48×10^{-6}	60	5
Liquid 2	1200	0.024	2×10^{-5}	65	5
Liquid 3	1200	0.46	3.83×10^{-4}	65	20

Table 1: Fluid properties for mass transfer for rising of single-component gas bubble

with the semi-analytical solution proposed by Fleckenstein and Bothe (2015), mass transfer from a rising bubble with no volume change and while forcing the species concentration in the bubble, and therefore the density, to remain constant is simulated until the barycentre of the bubble reaches (0 cm, 1.2 cm, 0 cm). The simulations are then restarted with local volume change taken into account.

For test case 2, the bubble size and computational domain remain the same, but the fluid properties are modified (Table 1) so that Eo=3 and Mo=10^{-5}. For these values, Clift's diagram (Clift *et al.*, 1978) predicts an ellispoidal shape. The bubble is initially at capillary equilibrium in the absence of gravity and interface mass transfer, with centre placed at (0 cm, 0.3 cm, 0 cm).

For test case 3, the domain considered and the gas bubble are five time larger (R=10 mm), and the bubble is immersed in liquid 3 (Table 1). The Eötvös and Morton numbers are 70 and 1.3, respectively. For these values, Clift's diagram (Clift *et al.*, 1978) predicts a dimpled ellipsoidal-cap shape. The bubble is initially at capillary equilibrium in the absence of gravity and interface mass transfer, with centre placed at (0 cm, 1.5 cm, 0 cm).

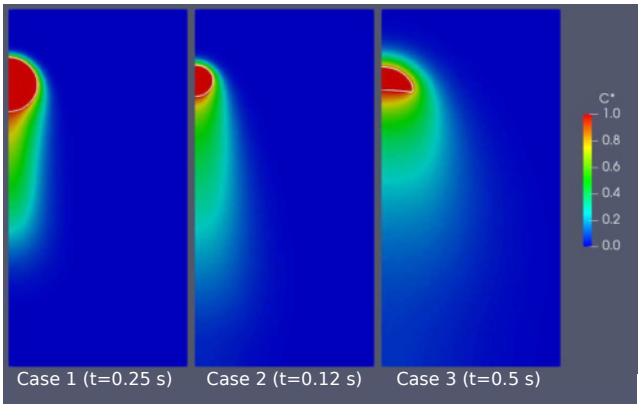

Figure 1: Numerical simulation of the dissolution of a rising bubble in liquid in the spherical regime (case 1), the ellipsoidal regime (case 2) and the dimpled ellipsoidal-cap regime (case 3). The colour represents the dimensionless solute component concentration and the white line the gas/liquid interface.

For each case, we perform eight simulations with four different mesh resolutions (75×150×75, 90×180×90, 120×240×120 and 150×300×150) and using the linear and the phase upwinding scheme. In Fig. 1, the color shows the dimensionless concentration of gas component in the domain, defined as

$$c^* = \frac{c}{\rho_g} \frac{H}{\alpha + H\,(1-\alpha)}. \tag{29}$$

at the end of the simulation, while the white line represents the gas bubble contour. In each case the bubble shape corresponds to the one predicted in Clift's diagram (Clift *et al.*, 1978).

Fig. 2, 3 and 4 show the evolution of the bubble mass for each simulation. For the spherical case (Fig. 2), the simulations are also compared with the semi-analytical solution (Fleckenstein and Bothe, 2015). We observe that the phase upwinding method always predicts more dissolution than the linear method. For the spherical bubble, both methods are first-order accurate, but the phase upwinding method seems

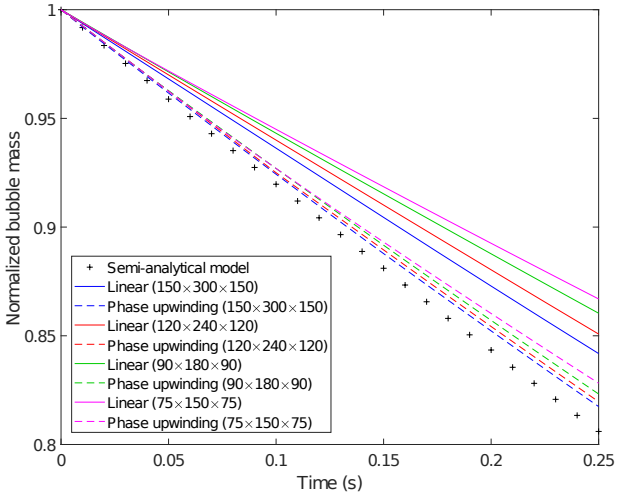

Figure 2: Evolution of bubble size obtained by semi-analytical solution and numerical simulations with various grid sizes and numerical schemes for test case 1 (spherical regime).

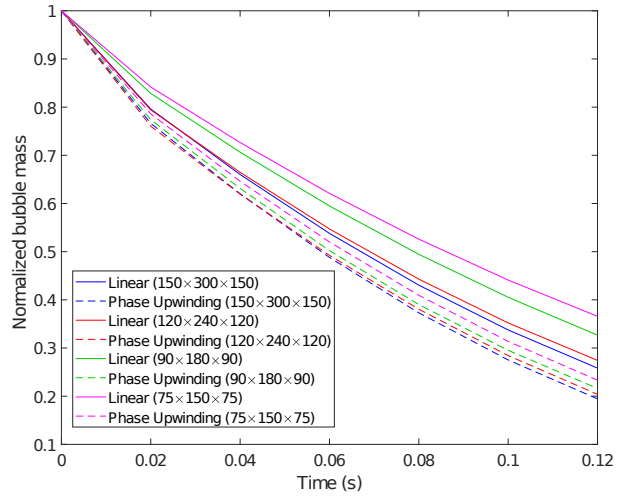

Figure 3: Evolution of bubble size obtained by numerical simulations with various grid sizes and numerical schemes for test case 2 (ellispoidal regime).

to be further in its convergence toward the semi-analytical solution. This suggests that the phae upwinding method is more accurate for all cases, so we will only use this method in the next example.

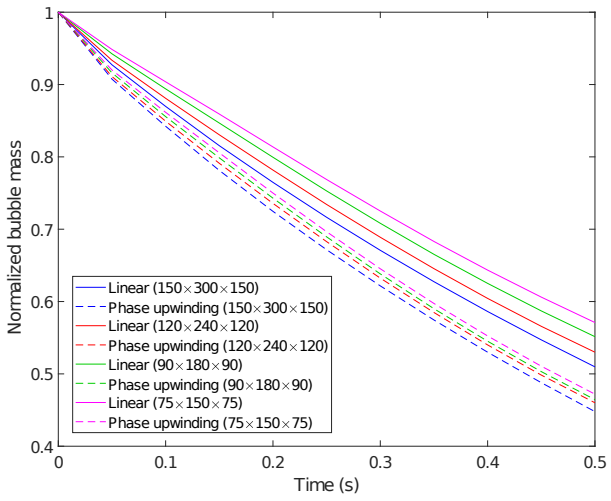

Figure 4: Evolution of bubble size obtained by umerical simulations with various grid sizes and numerical schemes for test case 3 (dimpled ellispoidal-cap regime)

CO_2 trapping

During Carbon Capture and Storage (CCS), clusters of CO_2 may remain trapped in the asperities of the solid surface after the pores are invaded by the water phase (Roman *et al.*, 2016). In this case, molecular diffusion, interface transfer, capillary forces and viscous dissipation all play a role in controlling the time-scale at which the CO_2 bubbles will dissolve in the water phase (Maes and Geiger, 2018; Roman *et al.*, 2019), a process known as solubility trapping.

In this part, we use our simulation framework to investigate mass transfer and dissolution in a pocket of residual CO_2 trapped in a cavity after water injection. The goemetry is a 6mm×1mm×1mm channel, with a 2mm×2mm×1mm cavity inserted in the middle (Fig. 5). Initially, CO_2 gas is trapped in the cavity and the rest is filled with water. The fluid properties are summarized in Table 2. At t=0, we inject water from the left boundary at two different speeds, 0.1 mL/min and 0.01 mL/min. These flow rates correspond to Peclet numbers Pe=104 and Pe=10.4, respectively.

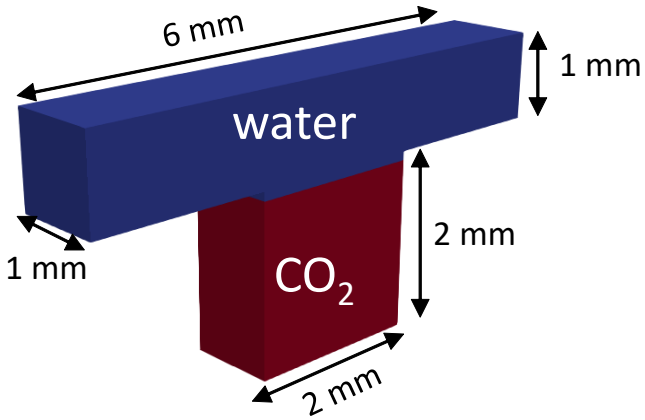

Figure 5: Schematic diagram of the cavity geometry and initial conditions

Fig. 6 shows a screenshot from the middle plan z=0 at different time for the two injection flow rates. The colour represents the single-field concentration of CO_2 and the white line the gas/liquid interface. We observe that at Pe=104, the transport of CO_2 in the water is mostly controlled by the advection, and the concentration of CO_2 follows a streamline around the bottom of the channel. However, for Pe=10.4, diffusion plays a more important role and the concentration of CO_2 is relatively large at any point dowmstream of the cavity.

Fig. 7 shows the evolution of the mass of the CO_2 bubble during the simulation for each Peclet number. For Pe=104, the slope of the curve does not change much and the dissolution remains close to linear. This is characteristic of an advection-dominated process, where the CO_2 in the water phase is flushed out of the domain rapidly and so does not impact the dissolution significantly. However, for Pe=10.4, we observe a transition between advection-dominated and diffusion-dominated regime, as the CO_2 accumulated at the interface by dissolution is not transported sufficiently fast and slow down the process. We conclude that CFD simulation using the VOF-CST metod can be applied to bring insights into the process of CO_2 solubility trapping during CCS in subsurface reservoir.

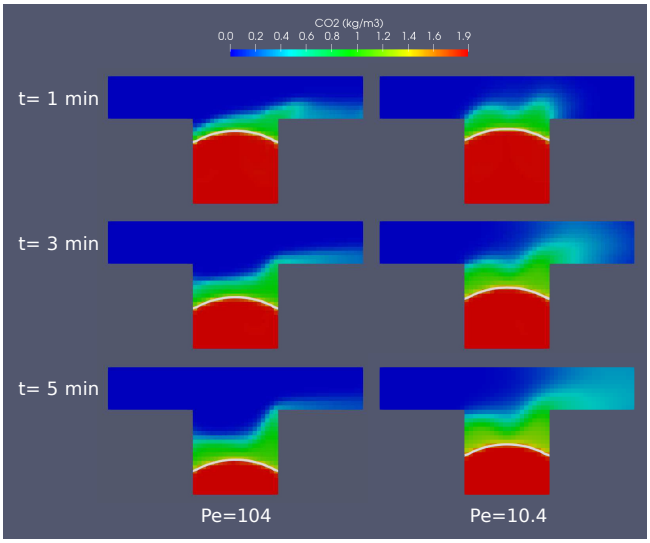

Figure 6: Numerical simulation of CO_2 dissolution in a cavity at two different Peclet numbers. The colour represents the single-field concentration of CO_2 and the white line the gas/liquid interface.

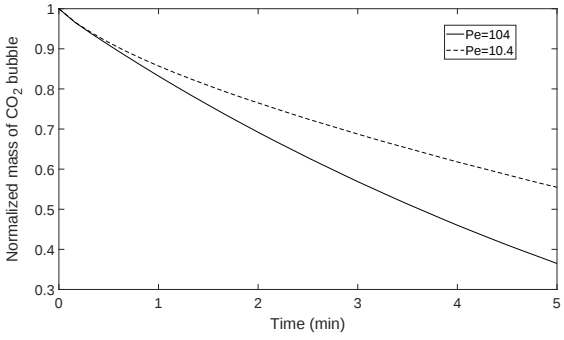

Figure 7: Evolution of the mass of a CO_2 bubble trapped in a cavity at two different Peclet number, obtained by numerical simulation.

	Density (kg/m^3)	Dynamic viscosity (Pa.s)	Diffusivity (m^2/s)	Interfacial tension (liquid-gas) (mN/m)	Henry's constant (no unit)
Gas	1.87	0.8×10^{-5}	0		
Liquid 1	1000	10^{-6}	1.6×10^{-9}	50	1.25

Table 2: Fluid properties for CO_2 dissolution in a cavity

CONCLUSION

In this paper, we used the VOF-CST method to numerically investigate the dissolution of a rising bubble in water at various regimes and the dissolution of a CO_2 bubble trapped in a cavity during injection of water in the subsurface. We compared results obtained with two different numerical discretizations of the interfacial fluxes for dissolution of a rising bubble in the spherical, ellipsoidal and dimpled ellipsoidal-cap regimes, and we concluded that the phase upwinding scheme was more accurate. We then emploied our simulation framework to investigate mass transfer and dissolution in a pocket of residual CO_2 trapped in a cavity after water injection at different flow rates and a transition from advection-dominated regime to diffusion-dominated regime was observed.

We conclude that our simulation framework can be used to investigate multiphase multicomponent reactive transport processes, and bring new insights into engineering application such as bubble reactors and CCS. In future work, we will employ the method to investigate the sensitivity of the process with respect to cavity sizes, shapes and number, as well as investigating the occurence of salt precipitation, a process known as mineral trapping.

REFERENCES

BRACKBILL, J.U., KOTHE, D.B. and ZEMACH, C. (1992). "A continuum method for modeling surface tension". *J. Comput. Phys.*, **100(2)**, 335–354.

CLIFT, R., GRACE, J.R. and WEBER, M.E. (1978). *Bubbles, drops, and particles*. New York; London: Academic Press.

DEISING, D., MARSCHALL, H. and BOTHE, D. (2016). "A unified single-field model framework for Volume-Of-Fluid simulations of interfacial species transfer applied to bubbly flow". *Chem. Eng. Sci.*, **139**, 173–195.

DEISING, D., BOTHE, D. and MARSCHALL, H. (2018). "Direct numerical simulation of mass transfer in bubbly flows". *Computer and Fluids*, **172**, 524–537.

FLECKENSTEIN, S. and BOTHE, D. (2015). "A volume-of-fluid-based numerical method for multi-component mass transfer with local volume changes". *J. Comput. Phys.*, **301**, 35–58.

FRANCOIS, J., DIETRICH, N., GUIRAUD, P. and COCKX, A. (2011). "Direct measurement of mass transfer around a single bubble by micro-plifi". *Chemical Engineering Science*, **66**, 3328–3338.

HAROUN, Y., LEGENDRE, D. and RAYNAL, L. (2010). "Volume of fluid method for interfacial reactive mass transfer: Application to stable liquid film". *Chem. Eng. Sci.*, **65(10)**, 2896–2909.

ISSA, R., AHMADI-BEFRUI, B., BESHAY, K. and GOSMAN, A. (1985). "Solution of the implicitly discretised reacting flow equations by operator-splitting". *J. Comput. Phys.*, **93(2)**, 388–410.

MAES, J. and GEIGER, S. (2018). "Direct pore scale reactive transport modelling of dynamic wettability changes induced by surface complexation in carbonate rocks". *Adv. iWater Resour.*, **111**, 6–19.

MAES, J. and SOULAINE, C. (2018). "A new compressive scheme to simulate species transfer across fluid interfaces using the volume-of-fluid method". *Chem. Eng. Sci.*, **190(23)**, 405–418.

MAES, J. and SOULAINE, C. (2020). "A unified single-field volume-of-fluid-based formulation for multi-component interfacial transfer with local volume changes". *J. Comput. Phys.*, **402(109024)**.

MARSCHALL, H., HINTERBERGER, K., SCHÜLER, C., HABLA, F. and HINRICHSEN, O. (2012). "Numerical simulation of species transfer across fluid interfaces in free-surface flows using OpenFOAM". *Chemical Engineering Science*, **78**, 111–127.

OPENCFD (2016). *OpenFOAM, the open source cfd toolbox, User Guide*. OpenCFD Ltd.

ROMAN, S., SOULAINE, C., ALSAUD, M.A., KOVSCEK, A. and TCHELEPI, H. (2016). "Particle velocimetry analysis of immiscible two-phase flow in micromodels". *Advances in Water Resources*, **95**, 199–211.

ROMAN, S., SOULAINE, C. and KOVSCEK, A. (2019). "Pore-scale visualization and characterization of viscous dissipation in porous media". *Journal of Colloid and Interface Science*, **558(269-279)**.

RUSCHE, H. (2002). *Computational fluid dynamics of dispersed two-phase flows at high phase fraction*. Ph.D. thesis, Imperial College London.

SOULAINE, C., ROMAN, S., KOVSCEK, A. and TCHELEPI, H.A. (2018). "Pore-scale modelling of multiphase reactive flow. application to mineral dissolution with production of co2". *J. Fluid Mech.*, **855**, 616–645.

UBBINK, O. and ISSA, R.I. (1999). "A method for capturing sharp fluid interfaces on arbitrary meshes". *J. Comput. Phys.*, **153**, 26–50.

VAN LEER, B. (1974). "Towards the ultimate conservative difference scheme. II. Monotonicity and conservation combined in a second-order scheme". *J. Comput. Phys.*, **14(4)**, 361–370.